Title:	Wavelet-based Islanding Detection in Grid-Connected PV Systems
Authors:	A. Pigazo, *Member, IEEE,* M. Liserre, *Senior Member, IEEE,* R. A. Mastromauro, *Student Member, IEEE,* V. M. Moreno, *Member, IEEE* and A. Dell'Aquila, *Member, IEEE*
Publication:	IEEE Transactions on Industrial Electronics, vol. 56, no. 11. November 2009. pp. 4445-4455.
D.O.I.:	10.1109/TIE.2008.928097

Wavelet-based Islanding Detection in Grid-Connected PV Systems

A. Pigazo, *Member, IEEE,* M. Liserre, *Senior Member, IEEE,* R. A. Mastromauro, *Student Member, IEEE,* V. M. Moreno, *Member, IEEE* and A. Dell'Aquila, *Member, IEEE*

***Abstract*—Distributed Power Generation Systems (DPGS) based on inverters require reliable islanding detection algorithms (passive or active) in order to determine the electrical grid status and operate the grid connected inverter properly. These methods are based on the analysis of the DPGS voltage, current and power in time or frequency domain.**

This paper proposes a time-frequency detection algorithm based on monitoring the DPGS output power considering the influence of the PWM, the output LCL filter and of the employed current controller. Wavelet analysis is applied to obtain time localization of the islanding condition. Simulation and experimental results show the performance of the proposed detection algorithm also in comparison with existing methods.

I. Introduction

A main issue associated to renewable energy sources connected to electrical grids through an active front-end is the proper operation of such grid interfaces in order to improve the power supply reliability and quality independently from the electrical characteristics of the renewable energy source and the grid conditions at the point of common coupling (PCC) [1]-[3]. The power converter topology [4]-[6], the controller structure, the supported functionalities and/or implementation issues [7] must be considered during the design process of the active front-end but, according to the international standards [8]-[15], the detection of the islanding condition must be also considered.

The islanding condition is defined in [8] and occurs when "a portion of the utility system that contains both load and distributed resources remains energized while it is isolated from the remainder of the utility system". In case of low-power *plug&play* PV systems, according to [12], the distributed resource must be stopped within 2 s of the formation of the unintentional island in order to avoid possible damages to local electrical loads or the PV inverter during the grid reconnection. Moreover, this condition can be mandatory in order to guarantee the safety of workers during maintenance operations of the electrical system [16].

The detection of the islanding condition is a classical issue in electrical engineering but it must be considered that in low power PV DPGS, where a minimum number of sensors is required to reduce the economical costs or, simply, load-side and grid-side sensors are not available, this condition must be determined from voltage and current measurements at the inverter-side of the PCC [17]. Wireless communication systems have decreased their cost and can be an alternative in future DPGS. Passive, active and hybrid detection methods have been proposed in literature as an alternative to grid-level detection methods.

Passive methods monitor the voltage and current at the inverter-side of the PCC. Measurements of the PCC voltage magnitude and frequency [18][19], harmonics [20] and phase [21] are considered, separately or simultaneously [22], in order to determine the islanding condition [23]. As a drawback, it must be considered that the proper operation of passive methods under all possible load, grid and DPGS powers can not be guaranteed [24]. The nondetection zone (NDZ) of each method [25] can be calculated in order to evaluate the detection techniques [26]. Moreover, it must be considered that grid voltage disturbances can cause the inopportune intervention of the anti-islanding algorithm during normal operation.

Active detection methods have been introduced as an alternative to passive methods. In this case, a controlled disturbance is introduced at the PCC and, when the islanding condition occurs, the disturbance force the detection method threshold [27][28] and, as a consequence, the NDZ is minimized or avoided. Diverse methods, such as impedance measurement or detetection [29]-[31], slip mode frequency shift (SMS)[32], active and reactive power variations [33] and active frequency drift (AFD)[34], have been proposed but, as drawbacks, they introduce a disturbance at the PCC and interaction between DPGS must be considered [35]. Hybrid methods combine the effectiveness of passive and active approaches and can be applied as alternative [36].

This paper extends the analysis given in [37] and proposes a wavelet-based detection method which can detect the islanding condition from local measurements of PCC voltage and current signals, as in case of passive methods, but evaluates the high-frequency components injected by the PV inverter, which depend on the characteristics of the employed pulse width modulator, LCL filter and current controller, to reveal the islanding condition, as done by active methods. As it will be shown, the spectrum of the PV inverter output power will suffer a small variation, after the islanding operation mode, over a continuous and relatively wide frequency band. Passive harmonic detection methods, based on DFT, doesn't allow these variations to be detected due to their low resolution, which depends on the number of selected harmonics. As a

A. Pigazo and V. M. Moreno are with the Dep. of Electronics and Computers, University of Cantabria, Santander, 39004 Spain (phone:+34-942-201338; fax: +34-942-201303; emails: pigazoa@unican.es, morenov@unican.es).

M. Liserre, R. A. Mastromauro and A. Dell'Aquila are with the Dep. of Electrical and Electronics Engineering, Polytechnic of Bari, Bari, 70126 Italy (emails: liserre@ieee.org, mastromauro@deemail.poliba.it, dellaqui@poliba.it).

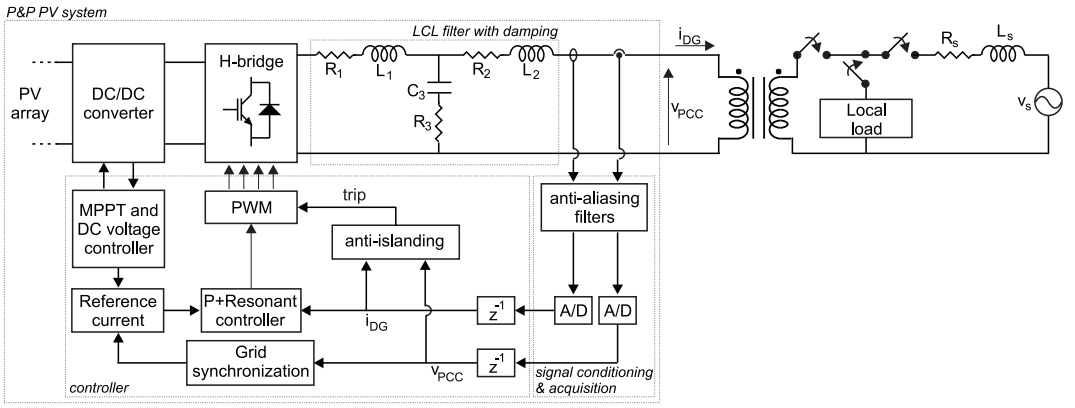

Fig. 1. Grid interface of the "plug&play" PV system under test according to IEEE Std. 1547.1 [13].

consequence, wavelet filter banks are proposed for tracking purposes of such spectrum variations in a properly selected frequency band. Section II shows the basis of the proposed method, including the procedure for selection of a suitable mother wavelet. Section III describes the selection method of proper detection levels and gives the NDZ of the proposed method and a comparison with two conventional detection methods. Section IV and V present the obtained experimental results and conclusions respectively.

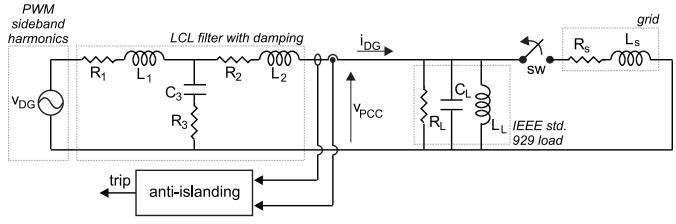

Fig. 2. Schematic of the high-frequency equivalent circuit.

II. Proposed detection method

The structure of a conventional inverter-based PV system is analyzed in this section. Special attention is given to the high-frequency behavior of the inverter output signals (voltage, current and power) and the impact of the PV inverter characteristics on these signals. This is the basis to propose an anti-islanding detection method using wavelet analysis and a methodology for a proper selection of a mother wavelet for islanding detection purposes.

A. Grid interface of a single-phase PV system

The general structure of a grid-connected PV system is shown in fig. 1. The DC/DC stage is operated using a Perturb & Observe (P&O) algorithm that adapts the voltage of the PV array in order to track the maximum power point (MPP) as temperature and irradiation change. Hence the MPPT computes the power that will be injected into the grid while the DC voltage controller adjust it in order to keep constant the dc voltage at the input of the H-bridge. Both MPPT and DC voltage controller contribute to determine the reference current, as reported in Fig. 1. The characteristics of the employed MPPT algorithm must be considered in order to evaluate the performance of the overall PV systems [38] but, due to the presence of the dc/dc converter, its impact on the performance of the anti-islanding algorithm can be neglected. The H-bridge is a full bridge. The ac peak voltage is $325\ V$. This voltage could be 15% higher [8]-[14], the grid filter can add a 10% voltage drop hence the ac voltage generated by the ac converter should be at least $406\ V$. Industrial inverters adopt a dc voltage $20\% - 50\%$ higher than this value in order to have safety margin. A signal conditioning and acquisition stage allows the output current i_{DG} and the PCC voltage v_{pcc} to be measured. A low-pass filter (LPF) is employed in order to avoid the aliasing effect associated to the acquisition of high frequency components in i_{DG} and v_{pcc} signals. The controller establishes the switching states of the grid-connected current-controlled single-phase inverter through a pulse width modulator. Sideband harmonics of the modulator carrier signal are minimized by introducing a LCL filtering stage properly designed [39]. The current controller is made by a proportional component and by a resonant term at the grid frequency. Details about the design process of this kind of controllers can be found in [40]. Three switches connected to the PCC allow islanding tests to be carried out according to IEEE Std. 1547.1 [13]. A test resonant load (R_L, C_L and L_L) with quality factor 1.25 has been considered during the islanding tests, both in simulation and experimentally, due to the laboratory restrictions. It must be considered that IEEE Std. 1547.1 suggests a quality factor equal to 1 [13].

Fig. 2 shows a simplified scheme, where the DPGS inverter has been modeled as a voltage source v_{DG} operating with multiple frequencies which depend on the employed pulse width modulation technique [41]. The LCL filter (R_1, L_1, R_2, L_2, R_3 and C_3) has been modeled considering ideal passive elements, R_s and L_s allows the effect of the grid impedance to be considered and the non-intentional islanding operation can be simulated by means of the switch sw. It must be considered that, once the islanding condition occurs, v_{DG} can suffer variations due to the dynamic characteristics of the grid synchronization algorithm included in the PV inverter

TABLE I
PARAMETERS OF THE ANALYZED PV SYSTEM

Parameter	Value	Parameter	Value
R_1, R_2	0.5 Ω	R_3	5 Ω
L_1	3 mH	L_2	1 mH
C_3	5 μF	C_L	37.6 μF
R_L	105.8 Ω	L_L	269.4 mH
L_s	2 mH	R_s	0.5 Ω
V_{dc}	600 V	$f_{carrier}$	6.4 kHz
P_{load}	500 W	Q_{load}	0 VA

controller.

B. Frequency behavior of the equivalent high-frequency PV system and basis of the proposed method

The frequency spectra of the output current i_{DG}, the PCC voltage v_{pcc} and the instantaneous output power p_{DG} signals have been measured through a simulation model matching the structure depicted in fig. 1. The grid interface of the PV system has been analyzed both in grid-connected and islanding operation modes. Table I shows the employed simulation parameters, which correspond to the worst case for passive anti-islanding detection methods ($P_{DG} = P_{load}$ and $Q_{DG} = Q_{load}$). The employed anti-aliasing filters are 2^{nd} order LPFs with $f_{carrier}/4$ cut-off frequencies. The LCL filter has been designed considering that the 1Φ DPGS inverter is controlled by means of a pulse width modulator which takes advantage of the unipolar modulation to reduce the weighted THD of i_{DG} [41]. The dc-bus voltage has been established at 600 V in order to ensure an appropriate current injection at the PCC trough the LCL filter but, in practical PV systems, this value should be properly adjusted in order to improve the overall performance.

The spectra of the measured signals, without the fundamental component, are shown in fig. 3. The employed base values are $V_{base} = 230\ V$, $I_{base} = 3.33\ A$ and $P_{base} = P_{load}$. Considering the PCC voltage, the inverter does not deteriorate the quality of the voltage waveform during the grid-connected operation (a 0.12 % VTHD) but, during the islanding operation, the distortion of the PCC voltage increases up to a 0.19 % (fig. 3.a). As it can be seen in fig. 3.b, the LCL filter attenuates the sideband harmonics of the pulse width modulator during the grid-connected operation and the total harmonic distortion (THD) of the i_{DG} signal is low (1.94 %) and within the limits established by IEEE Std. 929 [8]. The ITHD increases during the islanding operation mode reaching 3.52 %. The instantaneous output power p_{DG} consumption in grid-connected mode is carried out at the fundamental grid frequency but, during the islanding operation mode, other frequencies appear due to harmonics (fig. 3.c).

The dependency of v_{pcc}, i_{DG} and p_{DG} from v_{DG} during each possible operation mode at high frequency can be analyzed mathematically considering the circuit model shown in fig. 2. Due to the developed analysis, the effects of possible V_{DG} changes during the grid disconnection transient are neglected. From the complex impedances in fig. 2:

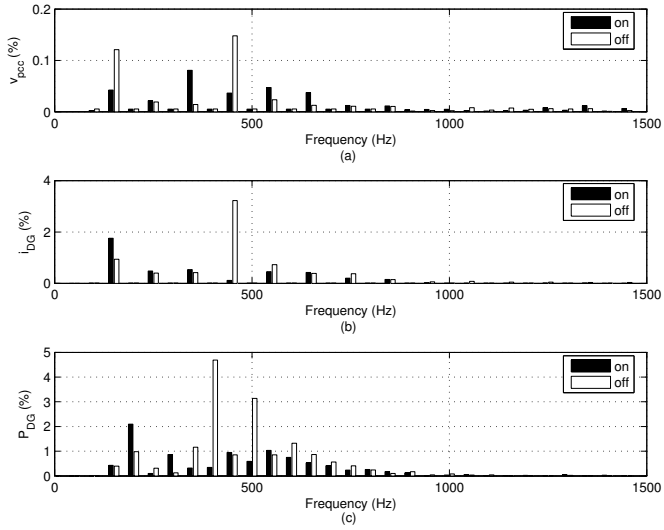

Fig. 3. Spectra of a) PCC voltage, b) DPGS output current and c) DPGS output power in grid-connected operation and disconnected.

$$Z_1(j\omega_{DG}) = R_1 + j\omega_{DG}L_1 \quad (1)$$

$$Z_2(j\omega_{DG}) = R_2 + j\omega_{DG}L_2 \quad (2)$$

$$Z_3(j\omega_{DG}) = \frac{j\omega_{DG}R_3C_3 + 1}{j\omega_{DG}C_3} \quad (3)$$

$$Z_L(j\omega_{DG}) = R_L // \frac{1}{j\omega_{DG}C_L} // j\omega_{DG}L_L \quad (4)$$

$$Z_S(j\omega_{DG}) = R_S + j\omega_{DG}L_S \quad (5)$$

result:

$$V_{pcc} = V_{DG}\frac{Z_3\left(Z_L//Z_S\right)}{Z_1Z_2 + Z_1Z_3 + Z_2Z_3 + \left(Z_1 + Z_3\right)Z_L//Z_S} \quad (6)$$

$$I_{DG} = \frac{V_{pcc}}{Z_L//Z_S} \quad (7)$$

$$P_{DG} = \frac{V_{pcc}^2}{Z_L//Z_S} \quad (8)$$

where P_{DG} is the frequency domain representation of the output power of the PV system corresponding to the baseband harmonics of the PWM carrier signal. Hence, the dependency of each magnitude from the DPGS voltage at each output frequency different from the fundamental component can be evaluated by means of:

$$\left|\frac{\partial V_{pcc}}{\partial V_{DG}}\right|_{on} = \left|\frac{Z_3\left(Z_L//Z_S\right)}{Z_1Z_2 + Z_1Z_3 + Z_2Z_3 + \left(Z_1 + Z_3\right)Z_L//Z_S}\right| \quad (9)$$

$$\left|\frac{\partial I_{DG}}{\partial V_{DG}}\right|_{on} = \left|\frac{1}{Z_L//Z_S}\right|\left|\frac{\partial V_{pcc}}{\partial V_{DG}}\right|_{on} \quad (10)$$

$$\left|\frac{\partial P_{DG}}{\partial V_{DG}}\right|_{on} = \left|\frac{2V_{DG}}{Z_L//Z_S}\right|\left|\frac{\partial V_{pcc}}{\partial V_{DG}}\right|_{on}^2 \quad (11)$$

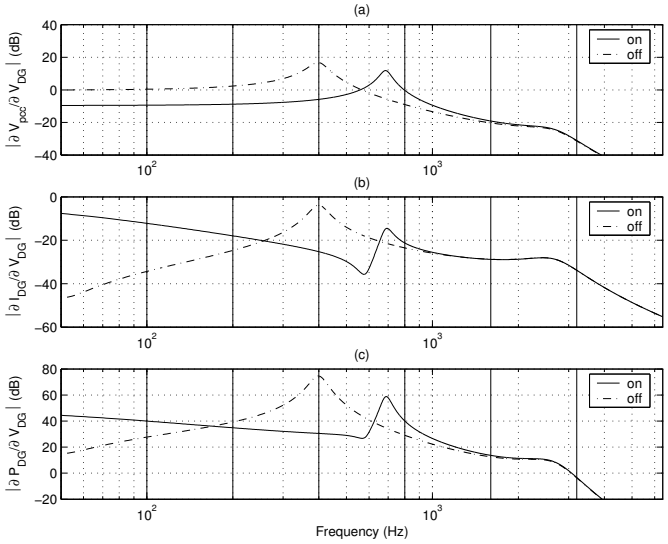

Fig. 4. Frequency response of the equivalent circuit at high frequency when the DPGS inverter is connected (on) and when it is not connected (off) to the grid.

where the subindex on denotes grid-connected operation. In order to minimize the effect of high frequency components of the PV system on the PCC voltage and current signals the output LCL-filter, Z_1, Z_2 and Z_3 must be properly designed [39]. The islanding operation mode can be analyzing by switching sw and, hence, (9)-(11) can be rewritten as:

$$\left|\frac{\partial V_{pcc}}{\partial V_{DG}}\right|_{off} = \left|\frac{Z_3 Z_L}{Z_1 Z_2 + Z_1 Z_3 + Z_2 Z_3 + (Z_1 + Z_3) Z_L}\right| \quad (12)$$

$$\left|\frac{\partial I_{DG}}{\partial V_{DG}}\right|_{off} = \left|\frac{1}{Z_L}\right| \left|\frac{\partial V_{pcc}}{\partial V_{DG}}\right|_{off} \quad (13)$$

$$\left|\frac{\partial P_{DG}}{\partial V_{DG}}\right|_{off} = \left|\frac{2V_{DG}}{Z_L}\right| \left|\frac{\partial V_{pcc}}{\partial V_{DG}}\right|^2_{off} \quad (14)$$

The frequency responses of (9)-(14) considering a conventional single-phase PV DPGS, parameterized in Table I, are shown in fig. 4. As it can be seen in fig. 4.a, the dependency of the PCC voltage from the DPGS output voltage, during grid-connected operation, is low but, once the islanding condition occurs, the PCC voltage is controlled by the DPGS inverter output voltage. The difference between gains reaches $22.76\ dB$ at $395.3\ Hz$. If the output current I_{DG} is considered (fig. 4.b) the difference reaches $37\ dB$ at $48.44 Hz$. Finally, analyzing the dependency of the DG output power P_{DG} from V_{DG} (fig. 4.c), a difference of $44\ dB$ is reached at $398.44\ Hz$. Hence, the greatest gain difference is reached considering (11) and (14).

According to the obtained results, the islanding-mode operation can be detected by measuring the amplitude variation of certain frequencies of the measured spectra $\left(\left|\frac{\partial V_{pcc}}{\partial V_{DG}}\right|, \left|\frac{\partial I_{DG}}{\partial V_{DG}}\right|, \left|\frac{\partial P_{DG}}{\partial V_{DG}}\right|\right)$. Depending on the number of resonant blocks, their frequency and the characteristics of the designed LCL filter, the frequencies which must be measured and the magnitude of the amplitude variations can be modified.

An operator $MA(f_s, f_e, S)$, where f_s and f_e are the starting and ending frequencies of the considered band and S is the frequency spectrum of the considered output signal (v_{pcc}, i_{DG} or p_{DG}), can be defined in order to determine the most appropriate frequency band and power signal for anti-islanding detection purposes:

$$MA(f_s, f_e, S) = \int_{f_s}^{f_e} \left(\left|\frac{\partial S}{\partial V_{DG}}\right|_{off} - \left|\frac{\partial S}{\partial V_{DG}}\right|_{on} \right) df \quad (15)$$

Applying this operator to the frequency bands and the power signals depicted in fig. 4, the Table II is obtained. Due to the fact that a higher value of MA implies a better resolution between both grid-connected and inslanding operation modes, the most appropriate output frequency bands in order to detect the islanding operation mode are the 4^{th} and 5^{th}. Moreover, the values in bold allows the best values for each output signal to be compared and, hence, P_{DG} has been selected for detection purposes. As a consequence, applying MA to the instantaneous output power of the PV system at 4^{th} and 5^{th} frequency bands, the islanding condition could be determined. However, time localization can not be achieved by applying (15).

C. Effects of the grid impedance on the PV system frequency response

According to (9)-(11), changes in the grid impedance would change the resolution at each frequency band and, as a consequence, the performance of the proposed method could be deteriorated. In order to analyze the impact of such grid impedance variations, Table II has been recalculated for 50% resistive and/or inductive variations. The obtained results, plotted as percentage of the nominal values (Table I), are shown in fig. 5 for 4^{th} and 5^{th} frequency bands. As it can be seen, the effect of the resistive variations (ΔR) is higher than the inductive ones and their impact depend on the analyzed output signal and frequency band.

Fig. 5.a and 5.b show the relative variation of the output of operator MA applied to V_{pcc} for the 4^{th} and the 5^{th} frequency bands. The maximum measured variations are 662.2 % and 33.7 % respectively. In case of I_{DG} (fig. 5.c and 5.d), the maximum variation is obtained at the 5^{th} frequency band (40.9 %) while the 4^{th} frequency band output remains below 33.3 %. The best measured results are obtained in case of P_{DG} at the 5^{th} frequency band, with a maximum variation of 13.5 % (fig. 5.f), while the measured value at the 4^{th} frequency band is 166.2 % (fig. 5.e).

From the analysis carried out up to this point, and applied to the PV system depicted in fig. 1, it can be established that the proposed anti-islanding detection method must track the 5^{th} frequency band in order to obtain the best possible resolution and independency from the characteristics of the PCC (grid impedance). However, the IEEE Std. 1547.1 [13] establishes that the islanding condition must be detected in less than 2 s, which can not be directly satisfied by applying (15) to the instantaneous output power of the PV inverter.

TABLE II
RESULTS OF $MA(f_s, f_e, S)$ APPLIED TO FIG. 4

Frequency band	1^{st} $f_e = 6400\ Hz$ $f_s = 3200\ Hz$	2^{nd} $f_e = 3200\ Hz$ $f_s = 1600\ Hz$	3^{th} $f_e = 1600\ Hz$ $f_s = 800\ Hz$	4^{th} $f_e = 800\ Hz$ $f_s = 400\ Hz$	5^{th} $f_e = 400\ Hz$ $f_s = 200\ Hz$	6^{th} $f_e = 200\ Hz$ $f_s = 100\ Hz$	7^{th} $f_e = 100\ Hz$ $f_s = 50\ Hz$
$MA\,(V_{pcc})$	-482.9 $dB \cdot Hz$	-910.9 $dB \cdot Hz$	-2401.1 $dB \cdot Hz$	-530.5 $dB \cdot Hz$	**3087.4** $dB \cdot Hz$	974.9 $dB \cdot Hz$	404.3$dB \cdot Hz$
$MA\,(I_{DG})$	-23.3 $dB \cdot Hz$	37.7 $dB \cdot Hz$	-224.0 $dB \cdot Hz$	**3033.7** $dB \cdot Hz$	1282.4 $dB \cdot Hz$	-1344.6 $dB \cdot Hz$	-1448.0 $dB \cdot Hz$
$MA\,(P_{DG})$	-506.2 $dB \cdot Hz$	-873.2 $dB \cdot Hz$	-2625.0 $dB \cdot Hz$	2503.2 $dB \cdot Hz$	**4369.9** $dB \cdot Hz$	-369.7 $dB \cdot Hz$	-1043.7$dB \cdot Hz$

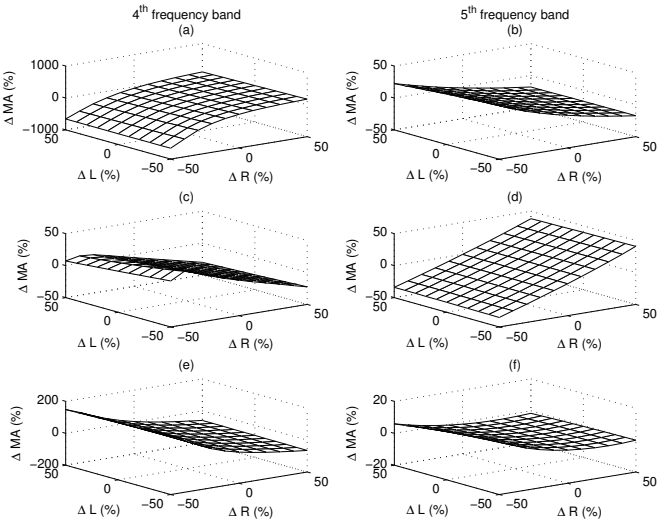

Fig. 5. Effect of grid impedance variations on islanding detection. a) 4^{th} frequency band and V_{pcc}, b) 5^{th} frequency band and V_{pcc}, c) 4^{th} frequency band and I_{DG}, d) 5^{th} frequency band and I_{DG}, e) 4^{th} frequency band and P_{DG} and f) 5^{th} frequency band and P_{DG}.

D. Wavelet analysis applied to the detection of the islanding condition in single-phase inverter based PV DPGS

In order to accomplish the time requirements in [13] it is proposed to apply the wavelet analysis to obtain time localization and tracking of a certain frequency band.

The Discrete Wavelet Transform (DWT) is a signal processing tool which can be applied when time-varying harmonics must be evaluated [42] and, as in the case of the detection of the islanding condition, time localization is required [43]. The DWT of a discrete function $x(k)$ can be defined as:

$$DWT(m,k) = \frac{1}{\sqrt{a_o^m}} \sum_n x(n)\psi\left(\frac{k - n a_o^m}{a_o^m}\right) \qquad (16)$$

where m and n are positive integers employed to define scaling and translating factors applied to the selected mother wavelet ψ. Due to the possible values of m, the frequency bands which can be measured by applying the DWT are logarithmic. These bands match the depicted ones in fig. 4. From this figure and, depending on the LCL-filter characteristics, the most suitable scale for islanding detection purposes can be selected. It must be considered that the response time of the anti-islanding detection algorithm will be shorter if a lower decomposition level is selected [44]. As a consequence, both the 4^{th} and 5^{th} decomposition levels have been selected. The

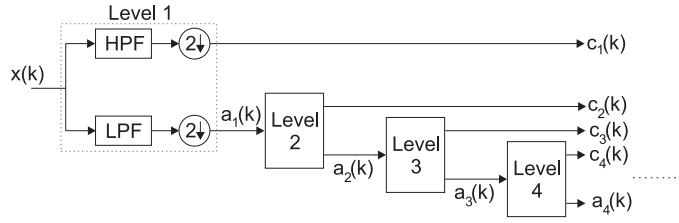

Fig. 6. Wavelet filter bank structure.

selection of the most appropriate mother wavelet is a key issue when applying the wavelet analysis and it will be discussed in following sections.

In order to simplify the detection algorithm implementation and tracking of the required frequency band, a filter bank structure, which is shown in fig. 6, has been selected [45]. The basic functional block corresponding to each decomposition level l is implemented by means of a high pass filter (HPF) $H(z)$, which generates the decomposition *details*, and a LPF $G(z)$, whose output corresponds to the decomposition *approximation*. The downsampling stages applied to the outputs of $H(z)$ and $G(z)$ are required in order to avoid information redundancy and obtain $c_l(k)$ and $a_l(k)$. It must be considered that the coefficients of $H(z)$ and $G(z)$ depend on the selected mother wavelet ψ and the logarithmic resolution required to establish the method frequency bands are due to the dyadic downsampling blocks. From the structure depicted in fig. 6 it is clear that the computational burden depends on the number of applied decomposition levels.

E. Mother wavelet selection

The performance of the proposed anti-islanding detection method relays on the selection of an appropriate mother wavelet ψ. 113 mother wavelets corresponding to Daubechies, Symlets, Coiflets, Biorthogonal and reverse Biorthogonal families have been tested on a simulation model corresponding to fig. 1 and considering the worst detection conditions ($\Delta P = \Delta Q = 0$). The wavelet filter bank structure depicted in fig. 6 has been applied to the instantaneous output power of the PV inverter. The variation of the signal *details* before and after the beginning of the islanding operation at the 5^{th} decomposition level (Δc_5) has been depicted in fig. 7 in order to determine the mother wavelet with best resolution. Pure sinusoidal and harmonically distorted grid voltages, according to IEEE Std. 519 (1^{st} 100%, 3^{rd} 2%, 5^{th} 2% and 7^{th} 4%, with $VTHD < 5\%$), have been applied to the simulation model.

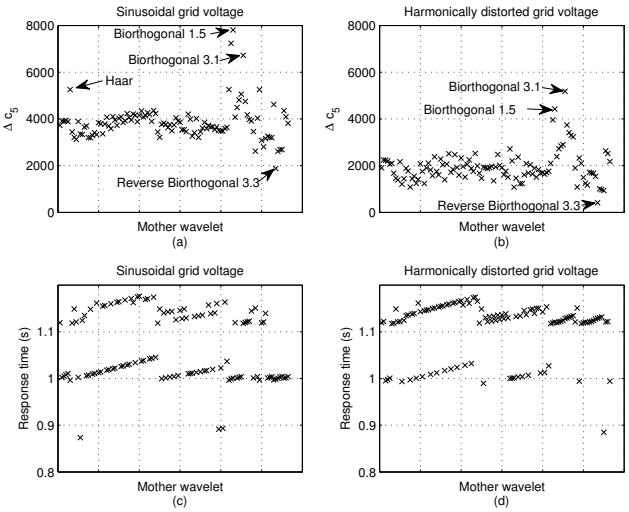

Fig. 7. 5^{th} decomposition level ($\Delta P = \Delta Q = 0$). *Detail* variations with a) pure sinusoidal and b) harmonically distorted grid voltages. c) and d) are the measured response times.

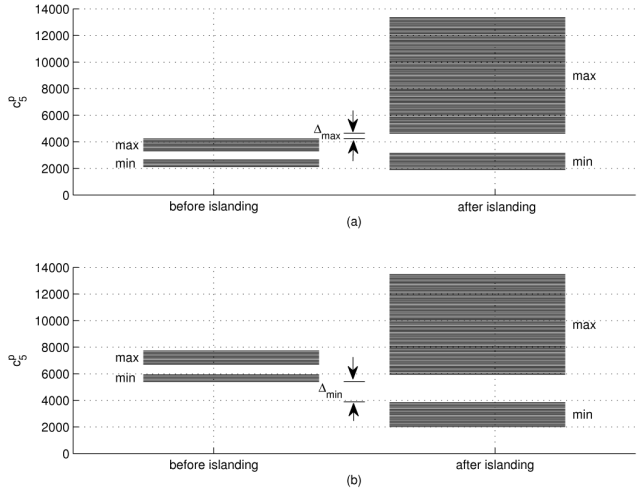

Fig. 8. Measured values of c_5^p inside the NDZ of passive methods for a) pure sinusoidal and b) harmonically distorted grid voltages. $\Delta_{max} = 399$ and $\Delta_{min} = 1534$.

From the obtained results at the 5^{th} decomposition level, the islanding operation mode is revealed in less than 2 s (IEEE Std. 1547.1) with both pure sinusoidal and distorted grid voltages. In case of sinusoidal grid voltages (fig. 7.a), the average value of the Δc_5 for the set of analyzed mother wavelets is 3852 while, in case of harmonically distorted grid voltages (fig. 7.b), this value reaches only 1945.9. From fig. 7.a, the mother wavelets with best resolutions are biorthogonal 1.5 and 3.1, which reach $\Delta c_5 = 7809$ and 6721 with response times (fig. 7.c) equal to $T_r = 0.8931\ s$ and $T_r = 1.118\ s$ respectively. Due to its implementation simplicity and the obtained results in case of sinusoidal PCC voltages, the Haar wavelet can be also considered as a good alternative ($\Delta c_5 = 5257$ and $T_r = 0.9966\ s$). It must be considered that the measured response times correspond to the time intervals between the beginning of the islanding operation mode and the maximum measured variation of c_5 and, as a consequence, the detection times can be improved by a proper selection of tripping levels. Equivalent results are obtained in case of harmonically distorted grid voltages, being biorthogonal 1.5 and 3.1 the best choices with $\Delta c_5 = 4420$ and $\Delta c_5 = 5183$ resolutions (fig. 7.b) and $1.119\ s$ and $1.128\ s$ response times (fig. 7.d) respectively. Considering the response times and the obtained resolution levels, the biorthogonal 1.5 has been selected for the implementation of the proposed anti-islanding detection algorithm.

F. Selection of detection levels

Once selected the most appropriate mother wavelet, the islanding condition can be detected by comparison of the measured peak values of c_5 and certain detection levels previously defined. As a consequence, a peak detector must be applied to c_5 each grid fundamental period:

$$c_5^p(k) = max\left(\mid c_5(k) \mid, \ldots \mid c_5(k-N+1) \mid\right) \qquad (17)$$

with N being the number of considered samples at the fundamental grid frequency. Fig. 8 has been obtained by applying (17) to the output of the wavelet filter bank structure and considering different output powers of the PV DPGS around P_{load} and Q_{load} (the applied maximum active and reactive power variations are 5% of the load power with 1% steps). As it can be seen, due to the employed ΔP and ΔQ, the maximum and minimum values of c_5^p before and after the islanding condition describe two bands whose characteristics depend on the employed LCL filter and the switching frequency of the PV inverter. It must be considered that the shown values of c_5^p, after the islanding condition, correspond to the measured values of c_5^p during the transient after the grid disconnection. The bands overlap once the steady-state is reached again.

The measured bands in case of pure sinusoidal pcc voltages are shown in fig. 8.a. As it can be seen, and considering the minimum measured values of c_5^p, the measured values before the islanding operation are inside the band obtained after the islanding condition but, in case of the maximum measured values, there is a distance $\Delta_{max} = 399$ between bands which allows a reliable detection after a rising crossing of a properly selected trip level T^H. In this case, it has been established adding $\frac{\Delta_{max}}{2}$ to the maximum measured value before the islanding operation.

The distribution of the measured maximum and minimum values of c_5^p changes in case of harmonically distorted grid voltages according to IEEE Std. 519 (fig. 8.b). In this case, the maximum measured values of c_5^p before the islanding condition are inside the measured band after the operation in electrical island but the minimum values present a gap equal to $\Delta_{min} = 1534$. From these results, a reliable detection of the islanding condition requires the comparison of the values obtained by applying (17) and two detection levels corresponding to sinusoidal and harmonically distorted grid voltages, T^H and T^L respectively. The PV inverter must be stopped if a raising crossing of T^H or a falling crossing of T^L occurs.

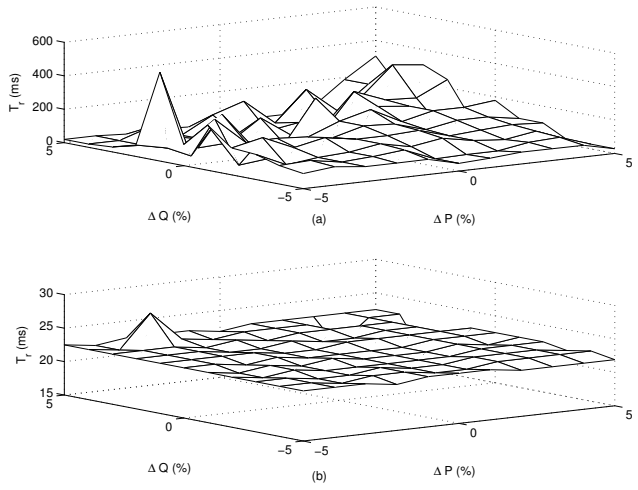

Fig. 9. Simulation results in case of a) pure sinusoidal and b) harmonically distorted grid voltages. $T^H = 4440$ and $T^L = 4655$.

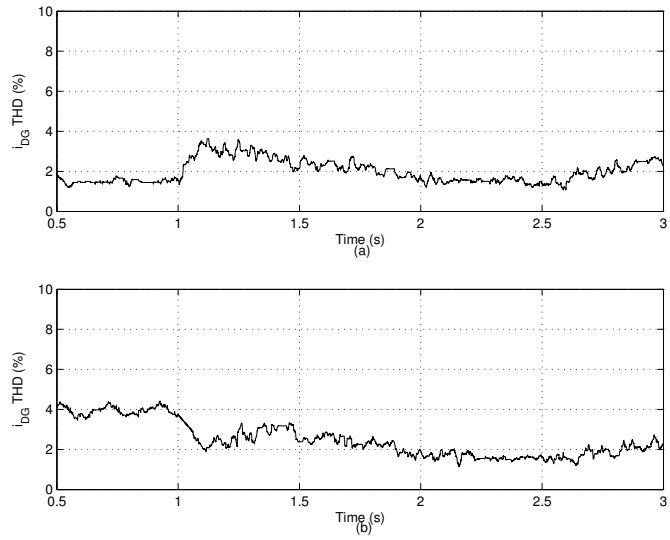

Fig. 10. Harmonic detection (HD) method. THD of i_{dg} with $P_{DG} = P_{load}$, $Q_{DG} = Q_{load}$. a) pure sinusoidal grid voltage and b) distorted grid voltage. The islanding operation occurs at $t = 1\ s$.

III. Simulation Results

The general structure shown in fig. 1 has been modeled and tested by means of MatLab/Simulink and the Power Systems BlockSet. The employed parameters have been shown in table I, the selected mother wavelet is a Biorthogonal 1.5 and the employed detection levels are $T^H = 4440$ and $T^L = 4655$. The designed anti-islanding detection method has been tested using pure sinusoidal and distorted grid voltages.

A. NDZ of the proposed method

The NDZ of the proposed method has been evaluated by applying the designed detection levels to the simulation model through c_5^p. The measured response times vary from half cycle at the fundamental grid frequency to 30 cycles (fig. 9.a) and within the range [17.19 ms, 26.87 ms] (fig. 9.b) in in case of pure sinusoidal and harmonically distorted grid voltages respectively. As a consequence, the islanding condition is properly detected according to [13] in both cases.

B. Performance comparison

The proposed wavelet-based detection technique has been compared to the Harmonic Detection (HD) [20] and Slip-Mode Frequency Shifting (SMS) [34] methods in order to evaluate their performances. The methods have been analyzed by simulation and implemented according to the general structure depicted in fig. 1.

The harmonic detection technique is a passive method which measures the THD of i_{DG} during the islanding test. Fig. 10.a shows the obtained results in case of a pure sinusoidal grid voltage. As it can be seen, the ITHD varies between 1.45%, in case of grid connected operation, and a maximum 3.59% measured at $t = 1.12\ s$. In order to detect the islanding condition, the detection level should be established within this range. Fig. 10.b shows the obtained results in case of harmonically distorted grid voltages. The THD varies within $[3.61\%, 4.39\%]$ during grid connected operation and falls to 1.50% after the islanding condition. Hence, the measured THD before the occurrence of the islanding condition depends on the harmonic distortion of the PCC voltage. Moreover, the obtained ITHD values have ripple which reduces the method resolution. As a consequence, a reliable detection level for all possible operation conditions and local loads can not be properly selected. The proposed wavelet-based method allows a reliable detection during all possible operation conditions (fig. 8) by selecting the most suitable frequency band for detection purposes. Moreover, from fig. 4, the resolution of the proposed method could be only reached by the harmonic detection technique by tracking all the harmonics inside the selected frequency band, which would increase the computational burden of the overall PV system controller.

In case of the SMS method, the phase angle of i_{DG} is dynamically changed depending on the measured mains frequency f_{DG}. Fig. 11.a and 11.c show the measured ITHD and f_{DG} in case of a pure sinusoidal grid voltage. f_{DG} is measured through the applied software phase-locked loop (SPLL) for synchronization purposes (fig. 1) and, as it can be seen in fig. 11.c, during the grid connected operation is maintained within [49.61 Hz, 50.37 Hz]. Once the islanding occurs, the positive feedback of this method forces the detection. It must be considered that the detection levels have been established at ± 1 Hz according to IEC 61727 [9]. From fig. 11.a and 10.a, this method increases the measured ITHD due to a higher instability caused by the positive frequency feedback [20]. In case of harmonically distorted grid voltages, f_{DG} is [48 Hz, 52 Hz] during grid connected operation due to the control characteristics of the employed SPLL. Diverse approaches can be applied for weakening of f_{DG} but, as consequence, the detection times and the overall complexity would increase, i.e. adding specifically designed algorithms for frequency measurement. From fig. 11.b, in grid connected

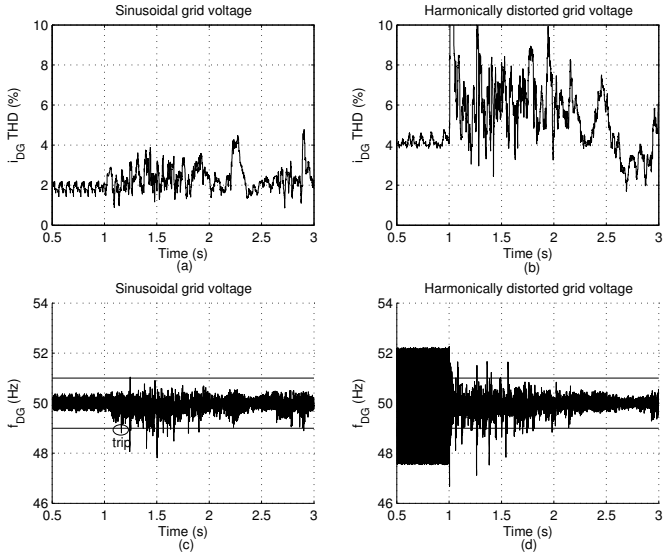

Fig. 11. Slip-Mode Frequency Shift (SMS) method with $P_{DG} = P_{load}$, $Q_{DG} = Q_{load}$. $i_{DG}THD$ with a) pure sinusoidal and b) harmonically distorted grid voltages. Measured frequency at the PCC (f_{DG}) in case of c) pure sinusoidal and d) harmonically distorted grid voltage. The islanding condition is applied at $t = 1\ s$.

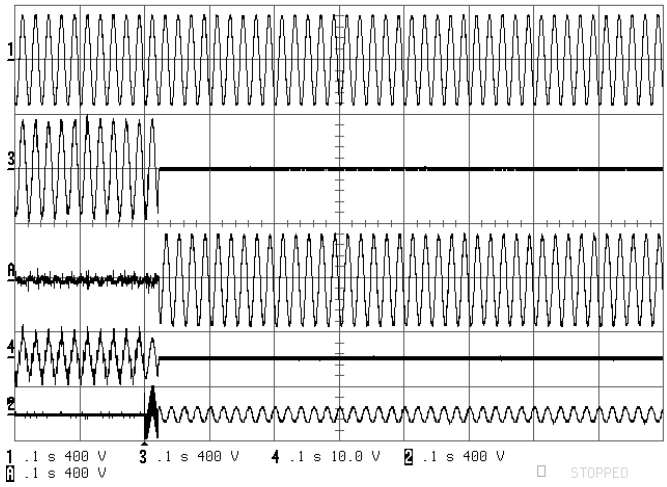

Fig. 12. Grid-disconnection transient in case of harmonically distorted grid voltage. Channel 1 is the measured grid voltage ($400\ V/div$). Channel 3 is the PCC voltage ($400\ V/div$). Channel A shows the difference between channel 1 and 3 ($400\ V/div$). Channel 4 is the inverter output current ($5\ A/div$). Channel 2 shows voltage across the switch which disconnects the isolation transformer.

operation, the ITHD increases due to the inherently instability of this method. From previous subsections, the inner structure of the proposed wavelet-based method, i.e. decomposition level for detection purposes, does not depend on the PCC conditions which are only considered for selection of most suitable detection levels (fig. 8). Moreover, the system stability is not affected by the proposed method.

IV. Experimental results

The proposed detection technique has been tested using an experimental setup where two controllable dc-sources $SM400$ from Delta Elektronika substitute the PV array and, as H-bridge, it is employed an ac motor drive $VLT - 5006$ from Danfoss, which has been modified by disabling the rectification stage and including a custom interface and protection card developed by Aalborg University (Denmark). Due to the fact the drive is 3ϕ, one leg of the IGBT-bridge remains stopped during the developed islanding tests. The PV system controller, which includes the proposed wavelet-based approach, is executed on a $DS - 1104$ control board from dSpace. The controller measures the inverter dc-voltage, the grid voltage and the inverter output current, which flows through the LCL filter, in order to determine the inverter switching status. An isolation transformer is connected between the electrical grid and the PV inverter. The PV system provides $P = 529\ W$ to the local load. The islanding condition can be generated by disconnecting the grid-side of the isolation transformer, which can be done by means of an available switch. Due to the characteristics of the developed setup, a low pass filter has been applied in order to smooth c_5^p values and, as a consequence, T^L has been changed to $770.^Q$ Three islanding tests have been carried out in order to evaluate the performance of the proposed controller under diverse operation conditions: distorted grid voltage, frequency variations and undervoltages.

Fig. 12 shows the obtained results in case of a harmonically distorted grid voltages according to the limits in IEEE Std. 519 (1^{st} 100%, 3^{rd} 2%, 5^{th} 2% and 7^{th} 4%), the measured VTHD is 4.89. Channel 1 shows the distorted grid voltage during the tests, with high 5^{th} and 7^{th} voltage harmonics. Once the islanding condition occurs at $0.2\ s$, the proposed method stops the PV inverter in less than 1 cycle at the fundamental grid frequency, as can be seen from channels 3, A, and 2. The output current, shown in channel 4, also drops to zero after the islanding condition.

A programmable power source has been employed in order to test the tolerance of the proposed method to grid frequency and voltage variations. The inner control variable Δc_5^p has been measured by means of the $ControlDesk$ software, from $dSpace$. Fig. 13.a shows the measured frequency during the first test, as it can be seen, $\pm 1\ Hz$ frequency steps are applied during 25 cycles at the fundamental grid frequency. The measured output current is shown in fig. 13.b. The SPLL, employed as grid synchronization mechanism, changes the frequency of the PV inverter reference current and the current controller tries to maintain the sinusoidal output current (during this test, the resonance frequency of the current controller depicted in fig. 1 is changed dynamically and considering the SPLL output). As it can be seen, the current waveform remains almost the same. The measured relative variations of c_5^p, depicted in fig. 13.c, show a correspondence between the output current waveform and Δc_5^p but the average value of Δc_5^p after the frequency step is -6.74%, which is not sufficient to trip the inverter.

The results of the voltage variations test are shown in fig. 14. As it can be seen in fig. 14.a, the amplitude of the applied grid voltage drop of 25% during the test. In order to maintain the

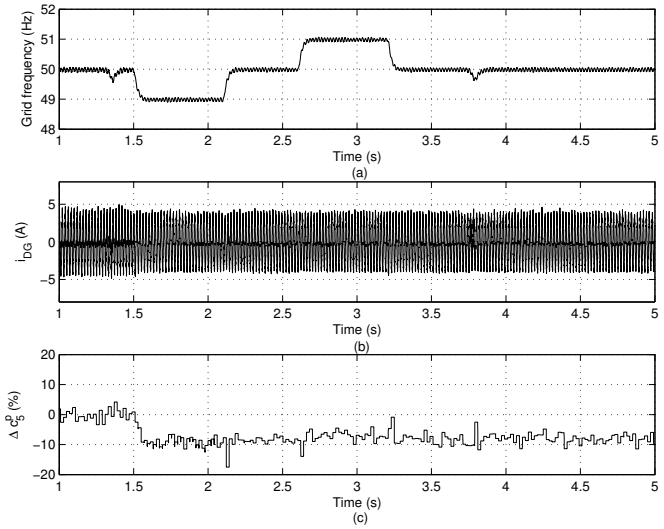

Fig. 13. Experimental tolerance test to frequency variations. a) The applied frequency variation, b) the measured output current and c) the variation of c_5^p during the test.

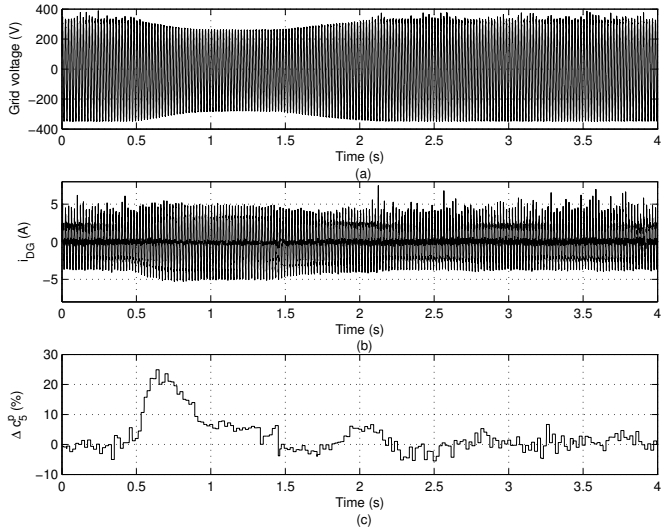

Fig. 14. Experimental tolerance test to voltage variations. a) The applied voltage variation, b) the measured output current and c) the variation of c_5^p during the test.

output power during the transient, the PV inverter generates an output current with higher magnitude (fig. 14.b). Due to the falling transient Δc_5^p reaches a 24% value, which could trip the PV inverter in case of very adjusted detection levels due to the dynamics of the applied overall controller. The second transient is slower and, as a consequence, the measured variation is lower, reaching a 6%.

V. Conclusions

This paper proposes a hybrid detection method which can detect the islanding condition from local measurements of PCC voltage and current signals, which are the basis of passive methods, but employs the high-frequency components injected by PV inverters, due to the applied pulse width modulator, LCL filter and current controller, to reveal the islanding condition. The proposed method takes advantage of time and frequency localization of the discrete wavelet transform (DWT) applied to the high-frequency components introduced by the DPGS inverter at the PCC. A theoretical analysis, the complete design process and the obtained results, both in simulation and experimentally, are given in this paper. The proposed method, which has been validated in presence of distorted grid voltages, frequency variations and undervoltages, is suitable for low-voltage low-power PV systems where a reduced number of sensors is available and the computational burden and complexity of the anti-islanding algorithm must be minimized.

Acknowledgment

This paper was partially supported by the Spanish Ministry of Science and Innovation under grant ENE2007-63979/ALT.

References

[1] J. M. Carrasco, L. G. Franquelo, J. T. Bialasiewicz, E. Galván, R. C. Portillo Guisado, M. A. M. Prats, J. I. Leon and N. Moreno-Alfonso, "Power-electronic systems for the grid integration of renewable energy sources: A survey," *IEEE Transactions on Industrial Electronics,* vol. 53, no. 4, June 2006. pp. 1002-1016.

[2] F. Blaabjerg, R. Teodorescu, M. Liserre and A. V. Timbus, "Overview of control and grid synchronization for distributed power generation systems," *IEEE Transactions on Industrial Electronics,* vol. 53, no. 5, October 2006. pp. 1398-1409.

[3] A. Kotsopoulos, P. J. M. Heskes and M. J. Jansen, "Zero-crossing distortion in grid-connected PV inverters," *IEEE Transactions on Industrial Electronics,* vol. 52, no. 2, April 2005. pp. 558-565.

[4] G. M. Martins, J. A. Pomilio, S. Buso and G. Spiazzi, "Three-phase low-frequency commutation inverter for renewable energy systems," *IEEE Transactions on Industrial Electronics,* vol. 53, no. 5, October 2006. pp.1522-1528.

[5] A. Alepuz, S. Busquets-Monge, J. Bordonau, J. Gago, D. González and J. Balcells, "Interfacing renewable energy sources to the utility grid using a three-level inverter," *IEEE Transactions on Industrial Electronics,* vol. 53, no. 5, October 2006. pp. 1504-1511.

[6] H. Ertl, J. W. Kolar and F. C. Zach, "A novel multicell DC-AC converter for applications in renewable energy systems," *IEEE Transactions on Industrial Electronics,* vol. 49, no. 5, October 2002. pp. 1048-1057.

[7] H. Koizumi, T. Mizuno, T. Kaito, Y. Noda, N. Goshima, M. Kawasaki, K. Nagasaka and K. Kurokawa, "A novel microcontroller for grid-connected photovoltaic systems," *IEEE Transactions on Industrial Electronics,* vol. 53, no. 6, December 2006. pp. 1889-1897.

[8] *IEEE Recommended Practice for Utility Interface of Photovoltaic (PV) Systems,* IEEE Std. 929-2000, 2000.

[9] IEC 61727 Draft, *Photovoltaic (PV) systems - Characteristics of the utility interface*.

[10] IEC 62116, *Testing procedure of islanding prevention measures for utility interactive photovoltaic inverters*.

[11] Standard VDE 0126-33, *Konzentrator-Photovoltaik (CPV)-Module und -Anordnungen Bauarteignung und Bauartzulassung,* (IEC 82/429/CDV:2006), Deutsche Fassung prEN 62108:2006 (in German).

[12] *IEEE Standard for Interconnecting Distributed Resources with Electric Power Systems,* IEEE Std. 1547-2003, July 2003.

[13] *IEEE Standard Conformance Test Procedures for Equipment Interconnecting Distributed Resources with Electric Power Systems,* IEEE Std. 1547.1-2005, July 2005.

[14] *IEEE Draft Application Guide for IEEE Standard 1547, Interconnecting Distributed Resources with Electric Power Systems,* IEEE P1547.2/D10, March 2008.

[15] *IEEE Guide for Monitoring, Information Exchange, and Control of Distributed Resources Interconnected with Electric Power Systems,* IEEE 1547.3, November 2007.

[16] R. A. Walling and N. W. Miller, "Distributed generation islanding-implications on power system dynamic performance," in *Proc. of 2002 IEEE Power Engineering Society Summer Meeting,* vol. 1, July 2002. pp. 92-96.

[17] M. E. Ropp, K. Aaker, J. Haigh and N. Sabbah, "Using power line carrier communications to prevent islanding [of PV systems]," in *Proc.* 28^{th} *IEEE Photovoltaic Spec. Conf.,* Sept. 15-22, 2000. pp. 1675-1678.

[18] S. Islam, A. Woyte, R. Belmans, P. Heskes, P. M. Rooij and R. Hogedoorn, "Cost effective second generation AC-modules: Development and testing aspects," *Energy,* vol. 31, no. 12, September 2006. pp. 1897-1920.

[19] J.-M. Kwon, K.-H. Nam and B.-H. Kwon, "Photovoltaic power conditioning system with line connection," *IEEE Transactions on Industrial Electronics,* vol. 53, no. 4, June 2006. pp. 1048-1054.

[20] V. Task, "Evaluation of islanding detection methods for photovoltaic utility-interactive power systems," Tech. Rep. IEA-PVPS T5-09:2002, December 2002.

[21] M. E. Ropp, M. Begovic, A. Rohatgi, G. A. Kern, R. H. Bonn, Sr., and S. Gonzalez, "Determining the relative effectiveness of islanding detection methods using phase criteria and nondetection zones," *IEEE Transactions on Energy Conversion,* vol. 15, no. 3, September 2000. pp.290-296.

[22] K. El-Arroudi, G. Joós, I. Kamwa and D. T. McGillis, "Intelligent-based approach to islanding detection in distributed generation," *IEEE Transactions on Power Delivery,* vol. 22, no. 2, April 2007. pp. 828-835.

[23] C. Jeraputra and P. N. Enjeti, "Development of a robust anti-islanding algorithm for utility interconnection distributed fuel cell powered generation," *IEEE Transactions on Power Electronics,* vol. 19, no. 5, Sept. 2004. pp. 1163-1170.

[24] M. Liserre, A. Pigazo, A. Dell'Aquila and V. M. Moreno, "An anti-islanding method for single-phase inverters based on a grid voltage sensorless control," *IEEE Transactions on Industrial Electronics,* vol. 53, no. 5, Oct. 2006. pp. 1418-1426.

[25] Z. Ye, A. Kolwalkar, Y. Zhang, P. Du and R. Walling, "Evaluation of anti-islanding schemes based on nondetection zone concept," *IEEE Transactions on Power Electronics,* vol. 19, no. 5, Sept. 2004. pp. 1171-1176.

[26] H. H. Zeineldin, E. F. El-Saadany and M. M. A. Salama, "Impact of DG interface control on islanding detection and nondetection zones," *IEEE Transactions on Power Delivery,* vol. 21, no. 3, July 2006. pp. 1515-1523.

[27] F. De Mango, M. Liserre and A. Dell'Aquila, "Overview of anti-islanding algorithms for PV systems. Part II: Active methods," in *Proc. of the* 12^{th} *International Power Electronics and Motion Control Conference (EPE-PEMC 2006),* Aug. 30^{th} - Sept. 1^{st} 2006. pp. 1884 - 1889.

[28] G.-K. Hung, C.-C. Chang and C.-L. Chen, "Automatic phase-shift method for islanding detection of grid-connected photovoltaic inverters," *IEEE Transactions on Energy Conversion,* vol. 18, no. 1, March 2003. pp. 169-173.

[29] A. V. Timbus, R. Teodorescu, F. Blaabjerg and U. Borup, "ENS detection algorithm and its implementation for PV inverters," *IEE. Proc.- Electr. Power Appl.,* vol. 153, no. 2, March 2006. pp. 206-212.

[30] C. Hernández González and R. Iravani, "Current injection for active islanding detection of electronically-interfaced distributed resources," *IEEE Transactions on Power Delivery,* vol. 21, no. 3, July 2006. pp. 1698-1705.

[31] L. Asiminoaei, R. Teodorescu, F. Blaabjerg and U. Borup, "Implementation and test of an online embedded grid impedance estimation technique for PV inverters," *IEEE Transactions on Industrial Electronics,* vol. 52, no. 4, August 2005. pp. 1136-1144.

[32] B. Yu, Y. Jung, J. So, H. Hwang and G. Yu, "A robust anti-islanding method for grid-connected photovoltaic inverter," in *Proc. of* 4^{th} *IEEE World Conference on Photovoltaic Energy Conversion, May 2006*. pp. 2242-2245.

[33] J. B. Jeong and H. J. Kim, "Active anti-islanding method for PV system using reactive power control," *Electronics Letters,* vol. 42, no. 17, August 2006. pp. 1004-1005.

[34] L. A. C. Lopes and H. Sun, "Performance assessment of active frequency drifting islanding detection methods," *IEEE Transactions on Energy Conversion,* vol. 21, no. 1, March 2006. pp. 171-180.

[35] H. H. Zeineldin, E. F. El-Saadany and M. M. A. Salama, "Islanding detection of inverter-based distributed generation," *IEE Proc.- Gener. Transm. Distrib.,* vol. 153, no. 6, pp. 644-652. November 2006.

[36] J. Yin, L. Chang and C. Diduch, "A new hybrid anti-islanding algorithm in grid connected three-phase inverter system," in *Proc. of* 37^{th} *IEEE Power Electronics Specialists Conference*, June 2006. pp. 1-7.

[37] A. Pigazo, V. M. Moreno, M. Liserre and A. Dell'Aquila, "Wavelet-based islanding detection algorithm for single-phase photovoltaic (PV) distributed generation systems," in *Proc. of IEEE International Symposium on Industrial Electronics,* June 2007, pp. 2409-2413.

[38] N. Femia, D. Granozio, G. Petrone, G. Spagnuolo and M. Vitelli, *Predictive & adaptative MPPT perturb and observe method,* IEEE Transactions on Aerospace and Electronic Systems, vol. 43, no. 3, July 2007. pp. 934-950.

[39] M. Liserre, R. Teodorescu and F. Blaabjerg, "Stability of grid-connected PV inverters with large grid impedance variation," in *Proc. of IEEE* 35^{th} *Annual Power Electronics Specialist Conference,* vol. 6, June 2004. pp. 4773-4779.

[40] R. Teodorescu, F. Blaabjerg, M. Liserre and P. C. Loh, "Proportional-resonant controllers and filters for grid-connected voltage-source converters," *IEE Proceedings-Electric Power Applications,* vol. 153, no. 5, Sept. 2006. pp. 750-762.

[41] D. G. Holmes and T. A. Lipo, *Pulse Width Modulation for Power Converters. Principles and Practice,* IEEE Press, 2003.

[42] V. A. Katic, J. M. Knezevic and D. Graovac, "Application-oriented comparison of the methods for AC/DC converter harmonics analysis," *IEEE Transactions on Industrial Electronics,* vol. 50, no. 6, December 2003. pp. 1100-1108.

[43] E. F. El-Saadany, T. K. Abdel-Galil and M. M. A. Salama, "Application of Wavelet transform for assessing power quality in medium voltage industrial distribution system," in *Proc. of 2001 IEEE/PES Transmission and Distribution Conference and Exposition,* vol. 1, 28 Oct.-2 Nov. 2001. pp. 427-432.

[44] S. Mallat, *A wavelet tour of signal processing,* 2^{nd} *ed.,* Academic Press, 1999.

[45] G. Strang and T. Nguyen, *Wavelets and filter banks,* 2^{nd} *ed.,* Wellesley College, 1996.

Alberto Pigazo (M'05) received the M.Sc. and Ph.D. degrees in physics (electronics) from the University of Cantabria, Spain, in 1997 and 2004, respectively.

Since October 2000, he has been teaching courses of electronics, power electronics and digital signal processing at the Dept. of Electronics and Computers of the same university, where he is currently an Assistant Professor. He has been a visiting researcher and professor at the Polytechnic of Bari, Italy. His main research interests include electrical power quality and digital signal processing techniques applied to the control of power converters.

Dr. Pigazo is member of the IEEE Industrial Electronics Society (IES) and the IES Technical Committee on Renewable Energy Systems (TCRES). He has been contributing for IEEE conferences and journals as author and reviewer.

Marco Liserre (S'00-M'03-SM'07) received the M.Sc. and Ph.D. degrees in electrical engineering from the Politecnico di Bari, Bari, Italy, in 1998 and 2002, respectively.

Since January 2004, he has been an Assistant Professor of power electronics, industrial electronics, and electrical machines with the Politecnico di Bari. He has been a Visiting Professor with Aalborg University, Aalborg East, Denmark, and he has been lecturing at different universities, including four tutorials at international conferences. He is a coauthor of 100 technical papers, 20 of which were published in international peer-reviewed journals, and three book chapters. His research interests include industrial electronics, with applications to distributed power generation systems based on renewable energies.

Prof. Liserre is a member of the IEEE Industrial Electronics Society (IES), IEEE Power Electronics Society, and IEEE Industry Applications Society. He has been a Reviewer for conference proceedings and journals for these societies. Within the IES, he has been actively responsible for student activities and Region 8 membership activities. He has also been a member of the Administrative Committee, an Editor of the newsletter, and the Chairman of the Technical Committee on Renewable Energy Systems. He has been involved in IEEE conferences organization in different capacities. He is an Associate Editor for the IEEE TRANSACTIONS ON INDUSTRIAL ELECTRONICS and the Editor-in-Chief of the *IEEE Industrial Electronics Magazine*.

Rosa A. Mastromauro (S'05) received the M.Sc. Degree in Electrical Engineering in 2005 from the Politecnico di Bari, where she is currently working toward the Ph.D. degree.

Since 2005 she has been with the Converters, Electrical Machines and Drives Research Team at the Politecnico di Bari. Her research activity concerns power converters control for distributed power generation systems based on renewable energies.

She is member of the IEEE Industrial Electronics Society, Power Electronics Society, Industry Applications Society, Women in Engineering Society and of the Italian Electrotechnical and Electronic Association (A.E.I.T.), she has been collaborating for IEEE Conference and journals as a reviewer.

Víctor M. Moreno (M'01) received the degree in physics (electronics) and the Ph.D. degree from the University of Cantabria, Cantabria, Spain, in 1980 and 1994, respectively.

He is currently an Associate Professor with the Department of Electronics and Computers, University of Cantabria. His research interests include electrical power quality, electromagnetic compatibility, digital signal processing, and digital control of power converters.

Prof. Moreno is member of the IEEE Power Electronics Society (PELS), was a recipient of the Viesgo Award, in 1994, for his Ph.D. thesis, entitled *Distributed System for the Measurement and Analysis of Electrical Power Quality Applying Kalman Filtering* and he has been collaborating for IEEE journals as a reviewer.

Antonio Dell'Aquila (M'87) received the M.Sc. degree in electrical engineering from the Università degli Studi di Bari, Bari, Italy, in 1970.

Since 1970, he has been with the Converters, Electrical Machines and Drives Research Team, Università degli Studi di Bari. He is currently a Full Professor of electrical machines, power electronics, and electrical drives with the Politecnico di Bari, Bari. He has published more than 100 technical papers on electrical machine models, transient analysis of rotating machines, inverter-fed induction machine performance, digital signal processing for nonsinusoidal waveforms, Kalman filtering for real-time estimation of induction motor parameters, and control, monitoring, and diagnostics of ac drives. His research interests include harmonic pollution produced by electronic power systems, PWM techniques for power converters, power converters in renewable energy conversion systems, active power filters, multilevel inverters, and intelligent control of power electronics equipment with fuzzy logic controllers.

Prof. Dell'Aquila is a member of the IEEE Power Engineering Society and the Italian Electrotechnical and Electronic Association.